T2R2 東京科学大学 リサーチリポジトリ
Science Tokyo Research Repository

論文 / 著書情報
Article / Book Information

Title	Soft Tensegrity Robot Driven by Thin Artificial Muscles for the Exploration of Unknown Spatial Configurations
Authors	Ryota Kobayashi, Hiroyuki Nabae, Gen Endo, Koichi Suzumori
Citation	IEEE Robotics and Automation Letters
Pub. date	2022, 2
Copyright	This work has been submitted to the IEEE for possible publication. Copyright may be transferred without notice, after which this version may no longer be accessible.
DOI	http://dx.doi.org/10.1109/LRA.2022.3153700
Note	This file is preprint version.

Powered by T2R2 (Science Tokyo Research Repository)

Soft Tensegrity Robot Driven by Thin Artificial Muscles for the Exploration of Unknown Spatial Configurations

Ryota Kobayashi[1], Hiroyuki Nabae[1], Gen Endo[1], and Koichi Suzumori[1]

***Abstract*—The primary role of a robot exploring an unknown space is to investigate the state and the spatial shape of the environment. We have designed a soft robot that aims to move forward in an unknown space as it recognizes and adapts to the spatial shape of the environment. We previously reported that soft tensegrity and recurrent neural network can be used to realize tensegrity structure shape recognition. In this study, a tensegrity robot was designed to actively generate propulsive force as it presses its body against a wall in its surrounding environment. This robot design includes a novel artificial muscle arrangement called "4/3 muscle winding," which induces large deformation in the tensegrity structure. The application of this new artificial muscle arrangement allows two types of large deformations to be induced in the tensegrity structure, which results in displacements of 20% to 40% in the axial and radial directions. We have demonstrated that the robot, which was created by connecting the tensegrity structures, is lightweight and possesses passive shape adaptability in a three-dimensional environment. This tensegrity robot could enter an unknown space, such as a cave, and recognize the spatial shape of the surrounding environment by recognizing the tensegrity structure shape.**

***Index Terms*—Soft robot applications, soft sensors and actuators, three-dimensional environment recognition, thin McKibben muscle, tensegrity structure**

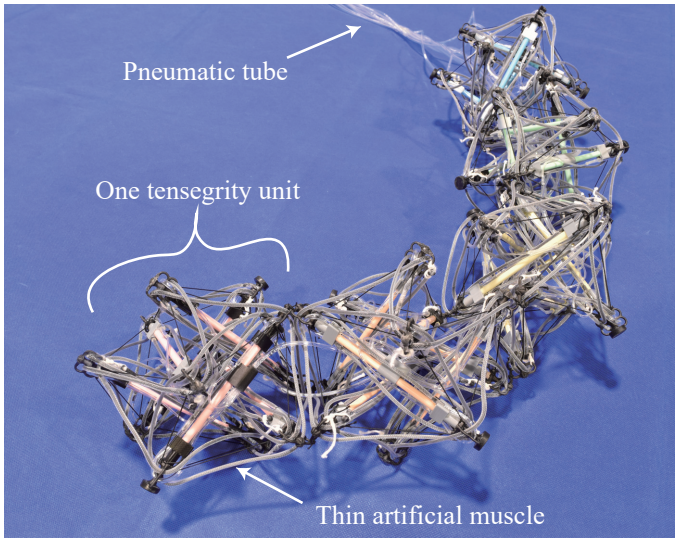


Fig. 1. Soft tensegrity robot driven by thin artificial muscles.

I. Introduction

ONE of the roles of robots is to explore unknown spaces that are inaccessible to humans. Some examples include the exploration of an environment with obstacles [1][2], and the exploration of an environment that cannot be directly observed [3][4]. In such an unknown space, one of the primary roles of a robot is to investigate the state and the spatial shape of the unknown environment. If the space is well lit, the robot can recognize the spatial shape of the environment by applying parallax triangulation in accordance with the structure-from-motion approach [5][6]. If the space is dark, the spatial shape of an object can be recognized by using time-of-flight sensors, such as light detection and ranging (LIDAR) and laser range finder (LRF) [7][8]. However, the optical and sonic echoes that are generally unavoidable in dark and narrow spaces makes it difficult to apply these methods to recognize the spatial shape of the environment.

A soft robot (e.g., [9][10][11][12]) can physically sense its surroundings in such an environment because of its passive shape adaptability to the external world. Thus, we purposed to realize a soft robot that can enter a space with an unknown spatial shape, and concurrently navigate through the space by utilizing wall-body contact, and recognize the 3D spatial shape of the space based on time-series data of its position and shape. Such a robot can be used, for example, for cave exploration and spatial shape recognition. In an unknown environment, the robot needs to be light enough to avoid disturbing the environment. For this reason, we focused on the development of a very light soft tensegrity structure driven by thin McKibben muscles [13], which have a large power output relative to their own weight and flexible movement among other lightweight artificial muscles [14]. We have previously reported on the success of tensegrity structure shape recognition by incorporating a soft thread sensor and processing the data using recurrent neural network (RNN) [15]. This allows the robot to recognize the spatial shape of the environment based on the knowledge of its own shape as it moves through a space with its body in contact with a wall assuming that the robot moves through a space of

Manuscript received: OCTOBER, 10, 2021; Revised JANUARY, 11, 2022; Accepted FEBRUARY, 8, 2022.

This paper was recommended for publication by Editor Kyu-Jin Cho upon evaluation of the Associate Editor and Reviewers' comments. This work was supported by JSPS KAKENHI Grant 18H05470.

[1]Ryota Kobayashi, Hiroyuki Nabae, Gen Endo, and Koichi Suzumori are with the Department of Mechanical Engineering, Tokyo Institute of Technology, 2-12-1 Ookayama, Meguro-ku, Tokyo 152-8550, Japan kobayashi.r.at@m.titech.ac.jp

Digital Object Identifier (DOI): see top of this page.

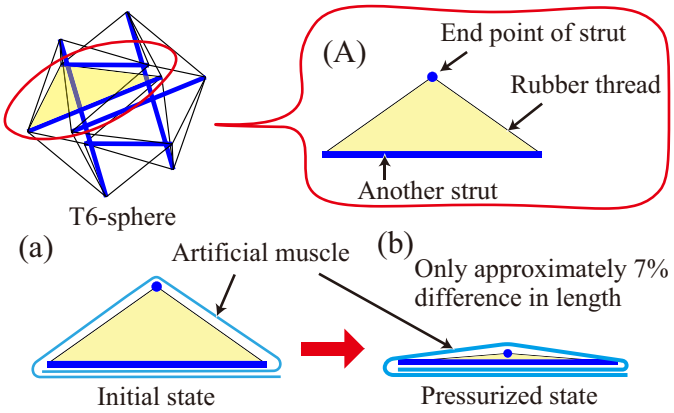


Fig. 2. Proposed 4/3 muscle winding scheme for the large deformation of tensegrity structures using artificial muscles.

the approximate size of the robot's motion range. However, a tensegrity robot that can move through an unknown space while adapting to the spatial shape of the environment has not been realized here.

For a body to make contact with a wall in an unknown space, it is necessary to realize a robot with a tensegrity structure that can undergo significant shape changes and apply moderate pressure against walls, which can be achieved via inchworm mechanisms. This mechanism requires the robot to generate a large amount of deformation in both the axial and radial directions. However, most of the tensegrity robots that have been developed to date deform a part of the structure to realize rolling motion under their own weight [16][17][18]. Such motion cannot actively generate horizontal or gravitational thrust, or passively adapt to the environment. Alternatively, robots that use artificial muscles to move tensegrity structures have also been studied [15][19][20][21], but the amount of deformation that they can achieve is insufficient for the desired motions. Thus, it is necessary to develop a new method that allows a large amount of displacement to be generated in the tensegrity structure using artificial muscles.

In this paper, we propose a new method for artificial muscle arrangement called "4/3 muscle winding;" this method enables large deformation in a one-unit tensegrity structure. The artificial muscle is flexible and can be activated in a bent position. Thus, it is possible to wind artificial muscles around the tensegrity structure using the proposed 4/3 muscle winding method; the amount of displacement of the entire structure can be increased without any additional mechanism. Additionally, by connecting the soft tensegrity structures that induce this large displacement, an inchworm robot was created, and its behavior was verified. Eventually, the robot will be able to enter into an unknown space and be able to recognize the spatial shape of its surrounding environment.

The remainder of this letter is organized as follows. In Section II, the design of a one-unit tensegrity structure that produces large deformations is described. Experiments on the environmental adaptability of the inchworm robot consisting of the tensegrity structures are described in Section III. Lastly, the conclusions and future plans are presented in Section IV.

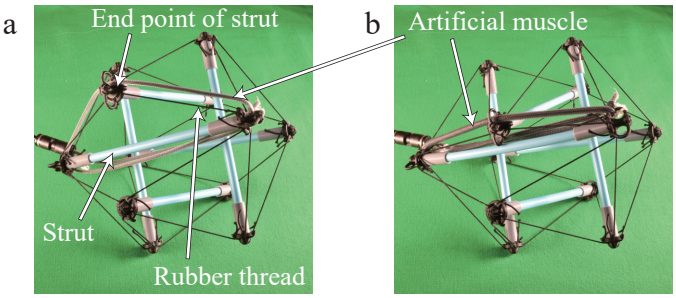


Fig. 3. Different states applied in the 4/3 muscle winding scheme: (a) initial state and (b) pressurized state.

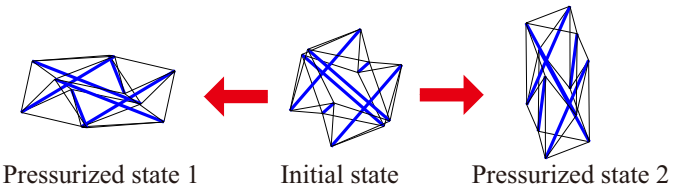


Fig. 4. Deformation induced by the artificial muscles.

II. Modeling and Design of Tensegrity Unit

This section describes 1) the concept of artificial muscle placement for the large deformation of tensegrity (i.e., Section II-A), and 2) the tensegrity model that induces large deformation (i.e., Section II-B). Then, in Section II-C, the effects of pre-stretching the rubber thread via simulation are discussed. For considering the effects of pre-stretching, the mathematical model is developed based on the potential energy of the system to deal with the balance of force; Section II-D discusses the experiments that were conducted using a real tensegrity structure.

A. Proposed 4/3 muscle winding concept

To begin, we will explain the concept of 4/3 muscle winding, which is a method that entails the arrangement of artificial muscles to significantly deform the tensegrity. In this study, a tensegrity structure called the T6-sphere was used; it consists of six struts and 24 rubber threads, as shown in Fig. 2. Our group has previously demonstrated that the shape recognition of tensegrity can be achieved by applying sensor threads as the rubber threads of the tensegrity [15].

In this tensegrity model, there are 12 strut endpoints, each of which has a isosceles triangle with itself as its vertex and another strut as the base as shown in Fig. 2(A).The triangle comprises two rubber threads and one strut. As shown in Fig. 2(a), the artificial muscles, which had a combined length of two struts and two rubber threads, was set to encompass the triangle. Thin McKibben muscles have a contraction ratio of approximately 20%; this means that two points that are connected by artificial muscles can only move toward each other by approximately 20%. However, by positioning the artificial muscles as shown in Figs. 2(a) and 3(a) and applying pneumatic pressure, it is possible to induce contact between the point and strut (i.e., a contraction ratio of 100%), as shown

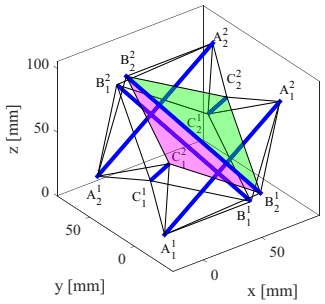


Fig. 5. Names and set variables for tensegrity vertices. The green triangle is Pattern 1 and the purple triangle is Pattern 2.

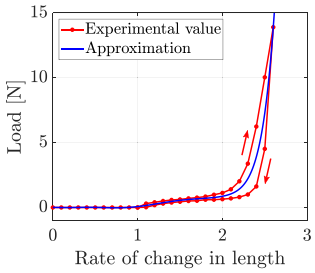


Fig. 6. Relationship between the rate of change in rubber length and load.

in Figs. 2(b) and 3(b). This is because the change in the length of the perimeter of the triangle is very small when it deforms (approximately 7%). Thus, the proposed 4/3 muscle winding method allows for 100% contraction ratio of distance between the point and the strut.

By applying 4/3 muscle winding to six of the 12 triangles in the tensegrity structure, the entire tensegrity structure can produce the two large deformations shown in Fig. 4.

B. Kinematics and statics

In the past, static [22] and dynamic analyses [23][24] and structural stability analyses [25][26] have been conducted for tensegrity structures. However, because the force of artificial muscles changes with displacement, it is necessary to consider the displacement in the analysis. Therefore, in this study, the conventional kinematic analysis of tensegrity is coupled with the displacement and force characteristics of the artificial muscles.

The name of each vertex in the tensegrity model was set as shown in Fig. 5, and the length of the strut was set to be L. In the event of stretching or shrinking along the z axis, the coordinates of the 12 vertices in the tensegrity model can be represented by only four variables, i.e., r, θ, ϕ, and h, according to the symmetry about the z-axis. The method is shown below.

First, let r be the length of one side of the triangle at the base, and denote the angles of the struts $\mathrm{A}_1^1\mathrm{A}_1^2$ using θ and ϕ, as follows:

$$\boldsymbol{A}_1^1 = (0,\ 0,\ 0)^\top, \tag{1}$$

$$\boldsymbol{B}_1^1 = (r,\ 0,\ 0)^\top, \tag{2}$$

$$\boldsymbol{C}_1^1 = \left(\frac{1}{2}r,\ \frac{\sqrt{3}}{2}r,\ 0\right)^\top, \tag{3}$$

$$\boldsymbol{A}_1^2 = (L\sin\theta\cos\phi,\ L\sin\theta\sin\phi,\ L\cos\theta)^\top. \tag{4}$$

Additionally, by setting h as the distance between bottom triangle $\mathrm{A}_1^1\mathrm{B}_1^1\mathrm{C}_1^1$ and top triangle $\mathrm{A}_2^2\mathrm{B}_2^2\mathrm{C}_2^2$, the center coordinates of the tensegrity model can be expressed as shown in Eq. (5).

$$\boldsymbol{P} = \left(\frac{1}{2}r,\ \frac{\sqrt{3}}{6}r,\ \frac{h}{2}\right)^\top \tag{5}$$

From the symmetry around the z-axis, using the rotation matrix $\boldsymbol{R}_\mathrm{z}(\theta)$ to rotate θ around the z-axis, the following relations are obtained.

$$\boldsymbol{B}_1^2 = \boldsymbol{R}_\mathrm{z}\left(\frac{2}{3}\pi\right)(\boldsymbol{A}_1^2 - \boldsymbol{P}) + \boldsymbol{P}, \tag{6}$$

$$\boldsymbol{C}_1^2 = \boldsymbol{R}_\mathrm{z}\left(\frac{4}{3}\pi\right)(\boldsymbol{A}_1^2 - \boldsymbol{P}) + \boldsymbol{P} \tag{7}$$

The coordinates of the remaining six vertices are then obtained from the symmetry about $\boldsymbol{P}$, as follows:

$$\boldsymbol{X}_2^i = 2\boldsymbol{P} - \boldsymbol{X}_1^{3-i} \quad (\boldsymbol{X} = \boldsymbol{A}, \boldsymbol{B}, \boldsymbol{C},\ i = 1, 2). \tag{8}$$

Then, the 12 vertices in the tensegrity model can be represented by using the four variables r, θ, ϕ, and h. Using the above-mentioned symmetry, the lengths of the 24 rubber threads can be partitioned into four categories. The four lengths are shown in Eq. (9), where $i = 1, 2$, and X and Y differ from each other in A, B, and C.

$$\left|\mathrm{X}_i^i\mathrm{Y}_i^i\right|,\ \left|\mathrm{X}_i^{3-i}\mathrm{Y}_i^i\right|,\ \left|\mathrm{X}_i^i\mathrm{Y}_{3-i}^i\right|,\ \left|\mathrm{X}_{3-i}^i\mathrm{Y}_i^{3-i}\right| \tag{9}$$

Let the names of the lengths given by Eq. (9) be, from left to right, $l_{\mathrm{rubber},1}$, $l_{\mathrm{rubber},2}$, $l_{\mathrm{rubber},3}$, and $l_{\mathrm{rubber},4}$. For example, $\mathrm{A}_1^2\mathrm{B}_1^1$ has i = 1, X = A, and Y = B, and is classified as $l_{\mathrm{rubber},2}$.

The potential energy is derived from the above-described variables. The shape of the tensegrity structure is calculated by solving the equilibrium equation, which is obtained by partial differentiation of the potential energy in each variable.

Because the tensegrity structure is sufficiently light, the total potential energy U of the model is expressed as the sum of the elastic energy of the rubber threads and the elastic energy of the artificial muscles. All properties of the rubber threads and artificial muscles used were measured by the tensile testing machine used at [27]. The measured value was an average value taken over five samples. The relationship between the length and load normalized by the natural length of the measured rubber thread is shown in Fig. 6. To simplify the analysis, hysteresis is ignored and the average value of loading and unloading is used. The function $f(l_\mathrm{rubber})$ of the load on the length l_rubber of the rubber thread is obtained by approximating to the 9th order function using the least-squares method. The highest order of the approximation function was set to the minimum value such that the norm of the error vector was less than 1% of the maximum value of the measurement.

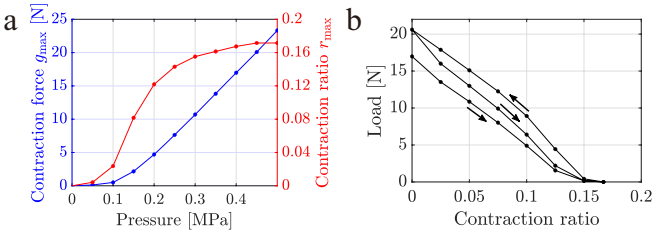


Fig. 7. (a) Artificial muscle contraction ratio and load as a function of pressure. (b) Relationship between the contraction ratio and load at P = 0.4 MPa.

The respective relationships between the pressure, load, and contraction ratio of an artificial muscle is shown in Fig. 7. It can be seen that the relationship between the load and contraction ratio can be linearly approximated when a pressure P is applied to the artificial muscle. Thus, the load applied to the artificial muscle when the length of the muscle is l_{muscle} can be obtained by using the contraction force $g_{\max}(P)$, contraction ratio $r_{\max}(P)$ when a pressure P is applied, and the length of the muscle $l_{\mathrm{muscle},0}$ when no pressure is applied, as follows:

$$g(l_{\mathrm{muscle}}) = \left(1 - \frac{l_{\mathrm{muscle},0} - l_{\mathrm{muscle}}}{r_{\max}(P) l_{\mathrm{muscle},0}}\right) g_{\max}(P). \quad (10)$$

By integrating the rubber thread load $f(l_{\mathrm{rubber}})$ and the artificial muscle load $g(l_{\mathrm{muscle}})$ with their respective lengths, the elastic energies of the rubber thread and artificial muscle can be respectively obtained as $F(l_{\mathrm{rubber}})$ and $G(l_{\mathrm{muscle}})$.

Two patterns of artificial muscle placement were considered. Pattern 1 entails the use of 4/3 muscle winding for triangle $\mathrm{A}_1^1\mathrm{A}_1^2\mathrm{B}_1^1$ and five other symmetrically positioned triangles. Pattern 2 entails the use of 4/3 muscle winding for triangle $\mathrm{A}_1^1\mathrm{A}_1^2\mathrm{B}_2^1$ and five other symmetrically positioned triangles. In the cases of Patterns 1 and 2, the artificial muscles are placed in relation to the z axis, so the tensegrity structure stretches and contracts along the z axis.

The length of an artificial muscle can be approximated according to the lengths of the two rubber threads and the two struts that form the enclosed triangle. For this reason, in the case of Pattern 1, the length of one artificial muscle can be approximated as the sum of the lengths of $|\mathrm{A}_1^1\mathrm{B}_1^1| = l_{\mathrm{rubber},1}$ and $|\mathrm{A}_1^2\mathrm{B}_1^1| = l_{\mathrm{rubber},2}$, and the combined length of two struts $2L$. Pattern 2 can be considered in the same way, and the length of one artificial muscle in Pattern k $(k = 1, 2)$ can be expressed as $l_{\mathrm{muscle},k} = 2L + l_{\mathrm{rubber},2k-1} + l_{\mathrm{rubber},2k}$. Thus, the total energy of the model can be expressed as the sum of the potential energy of the rubber threads, and the potential energy of the artificial muscles, as follows:

$$U_k(r, \theta, \phi, h) = 6 \sum_{i=1}^{4} F(l_{\mathrm{rubber},i}) + 6G(l_{\mathrm{muscle},k}), \quad (11)$$

where

$$F(l) = \int f(l)dl, \; G(l) = \int g(l)dl. \quad (12)$$

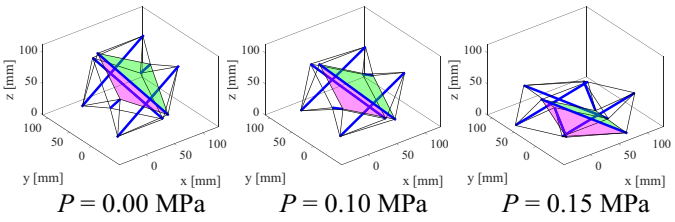


Fig. 8. Tensegrity model of Pattern 1 as the pressure is varied.

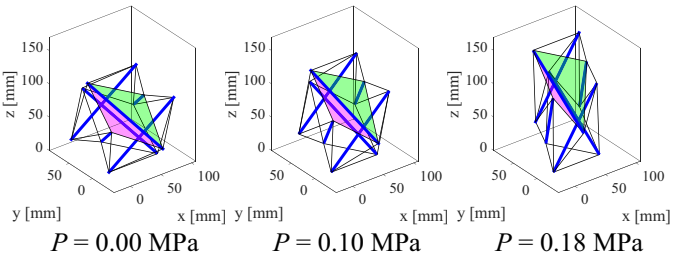


Fig. 9. Tensegrity model of Pattern 2 as the pressure is varied.

Partial differentiation of the potential energy obtained for each of the four variables yields equilibrium equations for each variable that can be obtained as shown in Eq. (13).

$$\frac{\partial U}{\partial r} = 0, \; \frac{\partial U}{\partial \theta} = 0, \; \frac{\partial U}{\partial \phi} = 0, \; \frac{\partial U}{\partial h} = 0 \quad (13)$$

Equation (13) can be solved numerically by using the MATLAB function (vpasolve), and this method is used for all simulations in this study. When L = 130 mm, the natural length of the rubber thread is 50 mm, and the artificial muscles follow Patterns 1 and 2, solving Eq. (13) leads to the deformation shown in Figs. 8 and 9. Artificial muscles are omitted for a clear understanding of the deformation of the structure.

In the case of Pattern 1, the deformation occurs as shrinkage along the z axis and extension in the radial direction; in the case of Pattern 2, the deformation occurs as extension along the z axis and shrinkage in the radial direction.

When applying the tensegrity structure to inchworm robots, it is desirable for one unit to be able to generate pulling and pushing forces that can be applied to other connected units. For this reason, artificial muscles were designed to be attached to Patterns 1 and 2. However, such conditions inhibit deformation because the length of the artificial muscles restricts movement. To solve this problem, the artificial muscles to be attached were made to be long and slack. Specifically, we attached an artificial muscle that was 1.1 times longer than the length of that shown in Fig. 2(a); we then confirmed that the deformation of the structure was not restricted by the length of the artificial muscle. In the simulation, when the artificial muscle is slack, the energy G of the artificial muscle should be set to zero.

C. Case studies for tensegrity design

As shown in Fig. 6, the rubber thread represents strong nonlinearity in the relationship between rate of change in length and load. So the natural length of the rubber thread is a

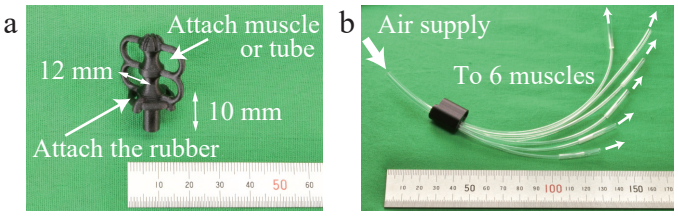


Fig. 10. (a) Component to be attached to the tip of the strut. (b) Fittings to split one tube into six tubes.

design parameter for tensegrity structure, which can affect performance of the tensegrity actuation. As mentioned above, our tensegrity robot requires large deformation in both the axial and radial directions, therefore, this Subsection investigates the effect of pre-stretching the rubber thread on the deformation of the tensegrity in each direction.

Figure 11 shows the variation of the structure of the rubber thread with respect to that at its natural length obtained from the simulation. The y-axis in Fig. 11 shows the ratio of the length at the steady state to the initial length in both the axial and radial direction of the tensegrity. In the actual tensegrity structure, a physical component shown in Fig. 10(a) at the vertices in the tensegrity structure come into contact with the strut, as shown in Fig. 3(b). Thus, the simulation was designed to terminate at the point where the distance between the struts equals 15 mm (i.e., 12 mm at the apex and 3 mm at the radius of the strut). When performing the actual length measurements for the tensegrity structure, the length of the component shown in Fig. 10 was also measured; this length was taken into account in the simulation.

In the simulation wherein 0.4 MPa was applied to the artificial muscle, the deformation of Pattern 1 did not significantly change when the natural length was at least 40 mm; alternatively, Pattern 2 most easily deformed when the natural length was approximately 50 mm.

D. Experimental evaluations

Each strut was made up of a 6-mm-diameter plastic rod with L = 130 mm; three bamboo sticks that were 110 mm in length and 2.5 mm in diameter were placed inside to prevent buckling due to compressive force. Rubber thread with the load displacements shown in Section II-B was also used. The rubber thread was fixed by attaching the component shown in Fig. 10(a) to the end of the strut. Regarding the role of this component, the artificial muscles were attached to three of the four holes, and a tube to be attached to the artificial muscles was passed through the remaining hole and then fixed. By using the pneumatic fitting shown in Fig. 10(b), we were able to ensure that the pneumatic pressure supplied from a single tube could be simultaneously applied to six artificial muscles. We used 1.8-mm-diameter tubes which have enough flexibility not to interfere with the deformation of tensegrity structure. The components shown in Fig. 10 were made using a 3D printer.

The effect of pre-stretching in II-C on the actual tensegrity structure is shown in Fig. 11. The amount of displacement

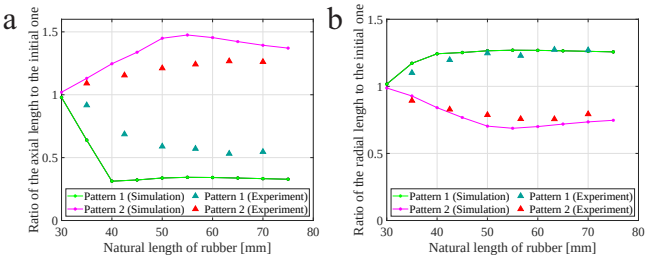


Fig. 11. Relationship between the natural length of the rubber thread and the ratio of (a) axial and (b) radial lengths to the initial ones when artificial muscles are placed in Pattern 1 and Pattern 2 and a pressure of 0.4 MPa is applied.

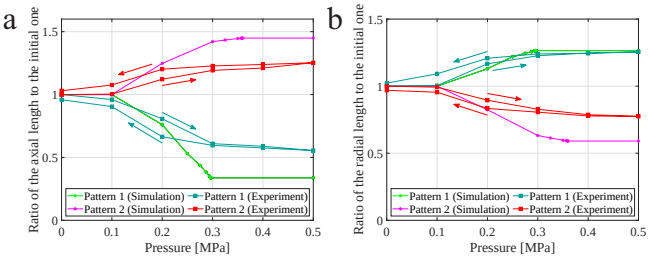


Fig. 12. Relationship between the applied pressure and the ratio of (a) axial and (b) radial lengths to the initial ones when the natural length of rubber thread is 50 mm.

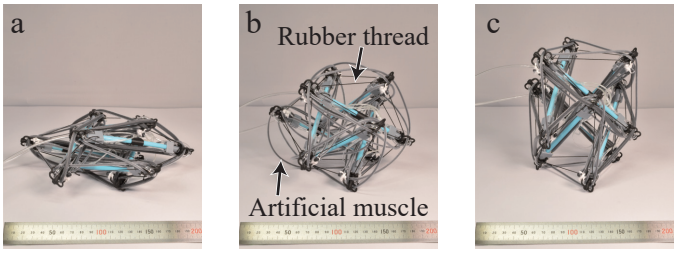


Fig. 13. (a) Tensegrity when artificial muscles are applied in Pattern 1. (b) Tensegrity in the initial state. (c) Tensegrity when artificial muscles are applied in Pattern 2.

was measured by placing two parallel plates on both sides of the deformed tensegrity structure and measuring the distance between them. The effects of pre-stretching on deformation, as described in Section II-C, are shown in Fig. 11 as a comparison between the simulation and experiment. When the deformation of the models was experimentally measured, there was no significant difference in the deformation mechanism when the natural length exceeded 50 mm.

According to [15], the shape of the tensegrity cannot be estimated if the rubber threads are slack. So the natural length of the rubber thread should be minimized. For this reason, a natural length of 50 mm is optimal, because it allows the tensegrity structure to be sufficiently deformed, while also discouraging rubber thread sagging.

Figure 12 shows the axial and radial length results for the tensegrity with a natural length of 50 mm. The tensegrity in this case is shown in Fig. 13. Pattern 1 resulted in a shrinkage of approximately 40% in the axial direction, and

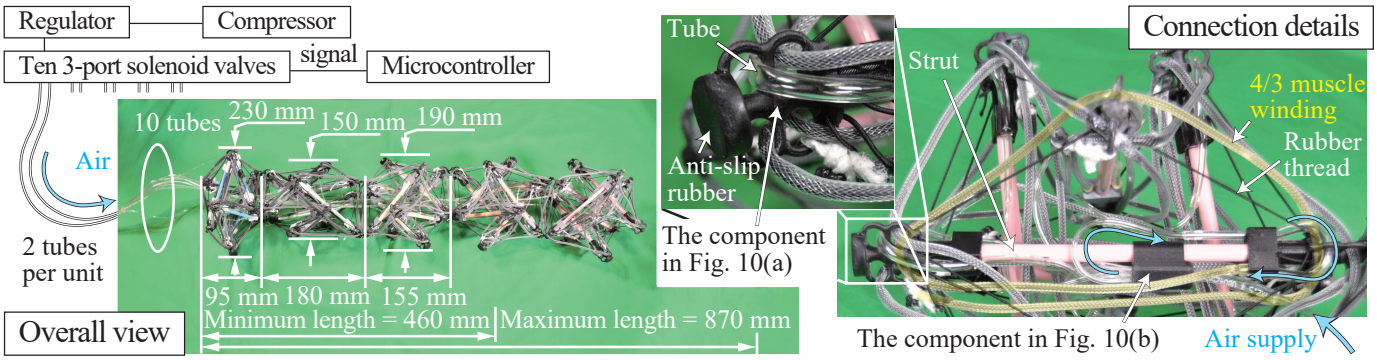


Fig. 14. Overall view of the tensegrity robot and the detail of the connection of the components.

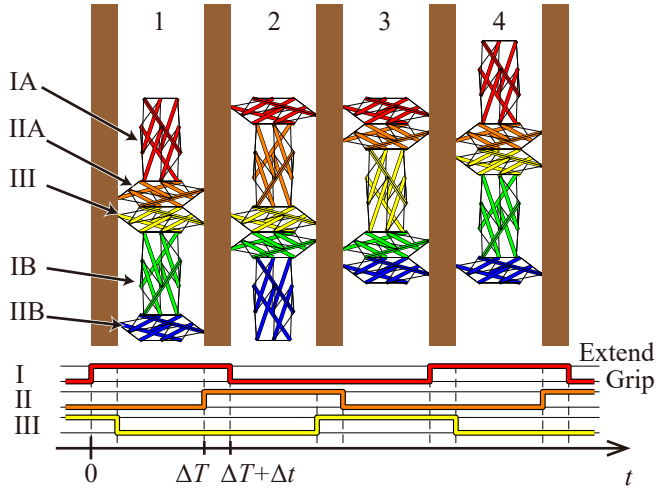


Fig. 15. Driving principle of the tensegrity robot and the control signal.

an elongation of approximately 25% in the radial direction. Pattern 2 resulted in approximately 25% elongation in the axial direction, and approximately 20% shrinkage in the radial direction. Consequently, a change from Pattern 1 to Pattern 2 resulted in 65% and 45% changes in the axial and radial directions. Application of the 4/3 muscle winding method can cause a large deformation to be generated in response to a very small change in the length of the artificial muscle; thus, it works well even when there is slack, and two patterns can be simultaneously implemented. A source of the discrepancies between the simulation and experiment is the large frictional force at the point where the artificial muscle bends. Because the large deformations in the two types of tensegrity structures that can be generated via 4/3 muscle winding significantly vary in the axial and radial directions, it should be possible to create an inchworm robot that propels by pushing its body against walls.

III. Design and Experimental Evaluation of Periodic Soft Tensegrity Robot

A. Robot design and control

By connecting the five tensegrity structures, an inchworm robot was created. The robot and its control system are shown in Fig. 14. For each unit, there are two sets of artificial muscles for Patterns 1 and 2 of the artificial muscle arrangement; thus, there are a total of 10 sets of artificial muscles in the five units. The control of these 10 pairs of artificial muscles occurs as follows. First, the pneumatic pressure from the compressor is adjusted to 0.4 MPa by the regulator. Then, five tensegrity deformations are controlled by using a microcontroller to control the on/off functionality of 10 3-port solenoid valves. By using this control system, the robot can move as shown in Fig. 15. The weight of the robot, excluding the pneumatic tubes, is 397 g. Additionally, to ensure that the robot grips the wall, we attached two anti-slip Tango Black rubber bumpers for each tensegrity that grips the wall, as shown in Fig. 14.

Figure 15 shows the driving principle of the robot. Each unit is named as shown in Fig. 15, the tensegrity robot moves in the direction opposite to the direction of the wave when it is moved for one cycle by changing the extending unit from Unit I→Unit II→Unit III while gripping the others.

B. Experimental evaluation

1) Spatial adaptability to path width: The influence of wall spacing on the driving characteristics of the robot was determined. Experiments were conducted to evaluate the movement of the robot when the distance between the walls was changed from 150 mm to 240 mm in 10-mm steps. Figure 16 shows how the robot moves when the wall-to-wall distances are 150, 200, and 240 mm. In each case, only the middle unit extends in the direction of motion, while the other units deform their tensegrity to grip the wall. Owing to its softness, the tensegrity robot is able to contact its body with a wall, even if the width between the walls changes. The speed at which the robot moves is shown in Fig. 17. To measure the speed, we performed the sequence shown in Fig. 15 ten times, and calculated the speed based on the distance traveled. The interval between each sequence was set to 2.0 s to allow sufficient deformation of the tensegrity structure.

When the wall spacing was 210 mm, the tensegrity structure was able to consistently establish contact with both sides of the wall; however, under the condition of wider spacing, the tensegrity robot was unable to consistently establish contact with the walls, as was observed in the case of the 240 mm spacing (Fig. 16). When the spacing between the walls was

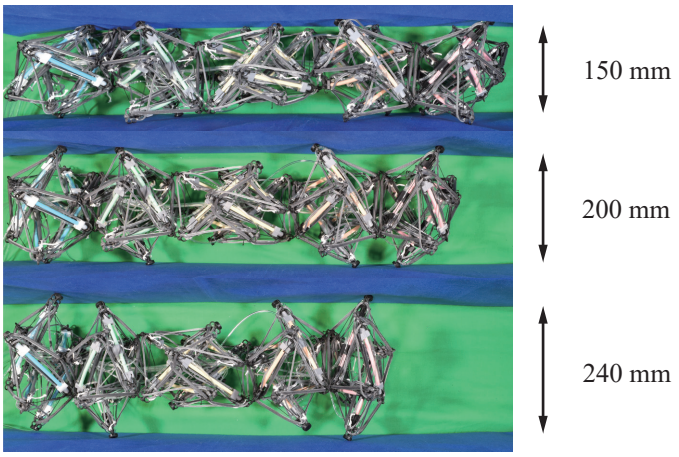


Fig. 16. Adaptation of the robot to the width of the wall.

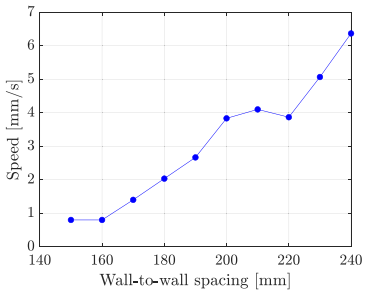


Fig. 17. Relationship between wall-to-wall spacing and speed.

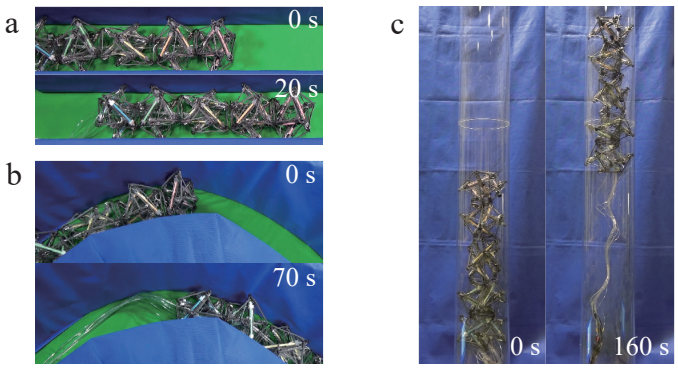


Fig. 18. (a) Moving along a straight path. (b) Moving along a curved path. (c) Vertical tube climbing demonstration.

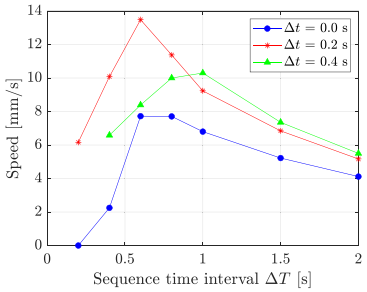


Fig. 19. Relationship between the sequence time interval ΔT and speed when the wall spacing is 210 mm.

narrow, the tensegrity structure deformed less in the radial direction; the extent of axial deformation also decreased accordingly; nevertheless, it was still able to move forward. In this case, the tensegrity structure was rotating with a slight twist in the axial direction.

2) Spatial adaptability to curved path: The adaptability of the curved environment is shown in Fig. 18, where Fig. 18(a) shows the robot moving along a straight path with a wall spacing of 210 mm; Fig. 18(b) shows the robot moving along a curved path with a radius of curvature of 550 mm and wall spacing of 210 mm. In both cases, the driving principle of the robot is the same, and the ΔT and Δt discussed in Section III-B4 were ΔT = 0.6 s, and Δt = 0.2 s. Under the condition of the same driving principle, the robot was able to passively adapt to even unknown environment.

3) Propelling forward in vertical pipe: The ability of the robot to overcome the force of gravity was also evaluated. When six anti-slip rubbers were attached to each unit, the robot was able to climb vertically through a pipe with an inner diameter of 210 mm, as shown in Fig. 18(c). However, under the condition of a relatively short time interval between sequences, the robot was occasionally unable to grip the pipe, which caused it to fall; this did not occur under the condition of horizontal movement. For this reason, the time interval of the sequence should be sufficiently long; thus, in the case of the movements shown in Fig. 18(c), ΔT = 1.0 s and Δt = 0.2 s were used. This experiment confirmed that, not only is the robot able to move along the horizontal plane, but it is also able to overcome the force of gravity. Thus, the robot is believed to be capable of such movements in an unknown environment, meaning that it should be able to adapt to and explore a 3D environment.

4) Driving frequency: Lastly, the influence of the time interval of the sequence on the driving characteristics of the robot was evaluated. The driving mechanism of this tensegrity robot differs from the conventional inchworm mechanism, in that its axial and radial motions are interlocked, which results in interference between them. For example, in Fig. 15-1→2, Unit I grips before Unit II is fully extended and the amount of extension of Unit II is reduced. For this reason, the gripping motion is delayed by Δt as shown in the control signal in Fig. 15. The change in the speed at which the robot moves in response to the change in the time interval of the sequence ΔT is shown in Fig. 19 for Δt = 0.0, 0.2, 0.4 s. The wall-to-wall distance was set to be 210 mm, and the sequence intervals were 0.2, 0.4, 0.6, 0.8, 1.0, 1.5, and 2.0 s. When the time interval was relatively long, the artificial muscles were able to sufficiently contract to deform the tensegrity; however, the speed of movement was slow because the time of one cycle was excessively long. Alternatively, when the time interval was relatively short, the speed was reduced because the artificial muscles did not sufficiently contract to deform the tensegrity. Under the conditions of Δt = 0.2 and 0.4 s, robot movement was faster than that which occurred under the condition of Δt = 0.0 s. Thus, unlike the conventional inchworm mecha-

nism, because the proposed inchworm mechanism mandates interlocking in the axial and radial directions, it is possible to ensure efficient movement by changing the timing of the application of pneumatic pressure.

IV. Conclusions

We have developed the 4/3 muscle winding method, which generates 100% collapsing motion under the conditions of a 20% artificial muscle contraction ratio; we also realized large deformation of the tensegrity structure. This method allows one tensegrity structure to perform the following two types of movements: 1) approximately 40% contraction in the axial direction and approximately 25% elongation in the radial direction under the conditions of an artificial muscle contraction ratio of approximately 20%, and 2) approximately 25% elongation in the axial direction and approximately 20% elongation in the radial direction.

By connecting the five units of the tensegrity structures, we were able to create a lightweight (approximately 400 g) tensegrity robot with passive environmental adaptability. The robot was demonstrated to be able to move between walls with widths ranging from 150 mm to 240 mm by adapting to its environment; it was also able to apply same driving method to move forward while adapting its body to a curved path with a radius of curvature of 550 mm. Furthermore, because the robot was able to climb a vertical pipe, it is expected that the robot will be able to adapt to and navigate complex 3D environments.

In the future, we plan to employ RNN to endow this tensegrity robot with the ability to recognize the spatial shape of an unknown environment.

References

[1] N. Keskın, E. Uslu, F. Çakmak, N. Altuntaş, M. F. Amasyali, and S. Yavuz, "Autonomous mobile robot exploration in negative obstacle environment," in *2017 25th Signal Processing and Communications Applications Conference (SIU)*, 2017, pp. 1–4.

[2] Y. Ozawa, M. Watanabe, K. Tadakuma, E. Takane, G. Marafioti, and S. Tadokoro, "Mono-wheeled flexible track capable of climbing high steps and adapting to rough terrains," in *2020 IEEE International Symposium on Safety, Security, and Rescue Robotics (SSRR)*, 2020, pp. 148–153.

[3] Y. Bando, T. Mizumoto, K. Itoyama, K. Nakadai, and H. G. Okuno, "Posture estimation of hose-shaped robot using microphone array localization," in *2013 IEEE/RSJ International Conference on Intelligent Robots and Systems*, 2013, pp. 3446–3451.

[4] Y. Bando, K. Itoyama, M. Konyo, S. Tadokoro, K. Nakadai, K. Yoshii, and H. G. Okuno, "Microphone-accelerometer based 3d posture estimation for a hose-shaped rescue robot," in *2015 IEEE/RSJ International Conference on Intelligent Robots and Systems (IROS)*, 2015, pp. 5580–5586.

[5] S. Ullman and S. Brenner, "The interpretation of structure from motion," *Proceedings of the Royal Society of London. Series B. Biological Sciences*, vol. 203, no. 1153, pp. 405–426, 1979. [Online]. Available: https://royalsocietypublishing.org/doi/abs/10.1098/rspb.1979.0006

[6] L. Torresani, A. Hertzmann, and C. Bregler, "Nonrigid structure-from-motion: Estimating shape and motion with hierarchical priors," *IEEE Transactions on Pattern Analysis and Machine Intelligence*, vol. 30, no. 5, pp. 878–892, 2008.

[7] Y. Cui, S. Schuon, D. Chan, S. Thrun, and C. Theobalt, "3d shape scanning with a time-of-flight camera," in *2010 IEEE Computer Society Conference on Computer Vision and Pattern Recognition*, 2010, pp. 1173–1180.

[8] J. Jimenez, M. Mazo, J. Urena, A. Hernandez, F. Alvarez, J. Garcia, and E. Santiso, "Using pca in time-of-flight vectors for reflector recognition and 3-d localization," *IEEE Transactions on Robotics*, vol. 21, no. 5, pp. 909–924, 2005.

[9] M. Takeichi, K. Suzumori, G. Endo, and H. Nabae, "Development of giacometti arm with balloon body," *IEEE Robotics and Automation Letters*, vol. 2, no. 2, pp. 951–957, 2017.

[10] S. Wakimoto, K. Ogura, K. Suzumori, and Y. Nishioka, "Miniature soft hand with curling rubber pneumatic actuators," in *2009 IEEE International Conference on Robotics and Automation*, 2009, pp. 556–561.

[11] M. M. Coad, R. P. Thomasson, L. H. Blumenschein, N. S. Usevitch, E. W. Hawkes, and A. M. Okamura, "Retraction of soft growing robots without buckling," *IEEE Robotics and Automation Letters*, vol. 5, no. 2, pp. 2115–2122, 2020.

[12] R. F. Shepherd, F. Ilievski, W. Choi, S. A. Morin, A. A. Stokes, A. D. Mazzeo, X. Chen, M. Wang, and G. M. Whitesides, "Multigait soft robot," *Proceedings of the National Academy of Sciences*, vol. 108, no. 51, pp. 20 400–20 403, 2011. [Online]. Available: https://www.pnas.org/content/108/51/20400

[13] S. Wakimoto, K. Suzumori, and J. Takeda, "Flexible artificial muscle by bundle of mckibben fiber actuators," in *2011 IEEE/ASME International Conference on Advanced Intelligent Mechatronics (AIM)*, 2011, pp. 457–462.

[14] W. Liang, H. Liu, K. Wang, Z. Qian, L. Ren, and L. Ren, "Comparative study of robotic artificial actuators and biological muscle," *Advances in Mechanical Engineering*, vol. 12, no. 6, p. 1687814020933409, 2020. [Online]. Available: https://doi.org/10.1177/1687814020933409

[15] W.-Y. Li, A. Takata, H. Nabae, G. Endo, and K. Suzumori, "Shape recognition of a tensegrity with soft sensor threads and artificial muscles using a recurrent neural network," *IEEE Robotics and Automation Letters*, vol. 6, no. 4, pp. 6228–6234, 2021.

[16] R. L. Baines, J. W. Booth, and R. Kramer-Bottiglio, "Rolling soft membrane-driven tensegrity robots," *IEEE Robotics and Automation Letters*, vol. 5, no. 4, pp. 6567–6574, 2020.

[17] K. Kim, A. K. Agogino, D. Moon, L. Taneja, A. Toghyan, B. Dehghani, V. SunSpiral, and A. M. Agogino, "Rapid prototyping design and control of tensegrity soft robot for locomotion," in *2014 IEEE International Conference on Robotics and Biomimetics (ROBIO 2014)*, 2014, pp. 7–14.

[18] K. Doney, A. Petridou, J. Karaul, A. Khan, G. Liu, and J. Rieffel, "Behavioral repertoires for soft tensegrity robots," in *2020 IEEE Symposium Series on Computational Intelligence (SSCI)*, 2020, pp. 2265–2271.

[19] Y. Koizumi, M. Shibata, and S. Hirai, "Rolling tensegrity driven by pneumatic soft actuators," in *2012 IEEE International Conference on Robotics and Automation*, 2012, pp. 1988–1993.

[20] S. Hirai and R. Imuta, "Dynamic simulation of six-strut tensegrity robot rolling," in *2012 IEEE International Conference on Robotics and Biomimetics (ROBIO)*, 2012, pp. 198–204.

[21] W.-Y. Li, H. Nabae, G. Endo, and K. Suzumori, "New soft robot hand configuration with combined biotensegrity and thin artificial muscle," *IEEE Robotics and Automation Letters*, vol. 5, no. 3, pp. 4345–4351, 2020.

[22] S. H. Juan and J. M. Mirats Tur, "Tensegrity frameworks: Static analysis review," *Mechanism and Machine Theory*, vol. 43, no. 7, pp. 859–881, 2008. [Online]. Available: https://www.sciencedirect.com/science/article/pii/S0094114X07001218

[23] H. Murakami, "Static and dynamic analyses of tensegrity structures. part 1. nonlinear equations of motion," *International Journal of Solids and Structures*, vol. 38, no. 20, pp. 3599–3613, 2001. [Online]. Available: https://www.sciencedirect.com/science/article/pii/S0020768300002328

[24] H. Murakami, "Static and dynamic analyses of tensegrity structures. part ii. quasi-static analysis," *International Journal of Solids and Structures*, vol. 38, no. 20, pp. 3615–3629, 2001. [Online]. Available: https://www.sciencedirect.com/science/article/pii/S002076830000233X

[25] G. Tibert and S. Pellegrino, "Review of form-finding methods for tensegrity structures," *International Journal of Space Structures*, vol. 18, pp. 209–223, 12 2003.

[26] C. Sultan and R. Skelton, "The prestressability problem of tensegrity structures: Some analytical solutions," *International Journal of Solids and Structures - INT J SOLIDS STRUCT*, vol. 38, 07 2001.

[27] S. Koizumi, S. Kurumaya, H. Nabae, G. Endo, and K. Suzumori, "Braiding thin mckibben muscles to enhance their contracting abilities," *IEEE Robotics and Automation Letters*, vol. 3, no. 4, pp. 3240–3246, 2018.